2014 IEEE Congress on Evolutionary Computation (CEC)
July 6-11, 2014, Beijing, China

Practical Application of an Evolutionary Algorithm for the Design and Construction of a Six-inch Submarine

Khairul Alam, Tapabrata Ray and Sreenatha G. Anavatti

***Abstract*— Unmanned underwater vehicles (UUVs) are becoming an attractive option for maritime search and survey operations as they are cheap and efficient compared to conventional use of divers or manned submersibles. Consequently, there has been a growing interest in UUV research among scientific and engineering communities. Although UUVs have received significant research interest in recent years, limited attention has been paid towards design and development of mini/micro UUVs (usually less than 1 foot in length). Micro unmanned underwater vehicles (μUUVs) are particularly attractive for deployment in extraordinarily confined spaces such as inspection of intricate underwater structures, ship wrecks, oil pipe lines or extreme hazardous areas. This paper considers previous work done in the field of miniature UUVs and presents an optimization framework for preliminary design of that class of UUVs. A state-of-the-art optimization algorithm namely infeasibility driven evolutionary algorithm (IDEA) is used to carry out optimization of the μUUV designs. The framework is subsequently used to identify optimal design of a torpedo-shaped μUUV with an overall length of six inches (152.4 mm). The preliminary design identified through the process of optimization is further analyzed with the help of a computer-aided design tool to come up with a detailed design. The final design has since then been built and is currently undergoing trials.**

I. Introduction

UNMANNED UNDERWATER VEHICLES (UUVs) are being widely used for a variety of applications ranging from environmental monitoring to oil and gas exploration [1]. The wide range of applications have resulted in development of hundreds of UUVs with a variety of shapes, sizes, working depth limits, sources of energy and means of propulsion [2]. Traditionally UUVs have tended to be large scale (meters in length) and high cost, making them unsuitable for small-scale environments [3].

Micro unmanned underwater vehicles (μUUVs) offer many advantages for performing difficult tasks submerged in water where larger scale UUVs fail to operate due to their shape and size constraints. Currently the μUUVs are being used for underwater archeology, geophysics and marine biodiversity investigation, exploitation of energy resources [4] and the mapping of nuclear storage ponds and wastewater treatment facilities [5]. In most cases, the μUUVs provide an added benefit of conducting various operations for a greater time period and with less risk relative to the alternative of manned underwater vehicles or commercial divers.

Some recent works dedicated to the design of μUUVs are [6]–[12]. The vast majority of the above listed works have focused on functional design. Very limited research has been directed to identify optimum designs. Alam *et al.* [2] carried out a design optimization process for an existing model submarine to observe the benefits of such a technology. The study identified a design with lower drag and better performance while accommodating all its internal components in a clash free state.

Khairul Alam, Tapabrata Ray and Sreenatha G. Anavatti are with the School of Engineering and Information Technology, The University of New South Wales, UNSW Canberra, ACT 2600, Australia (email: {k.alam, t.ray, s.anavatti}@adfa.edu.au).

In this paper, we use the optimization framework to develop the concept and preliminary design of a six inch submarine. The optimum design is subsequently analyzed to develop a detailed design which is eventually built. The objective of the optimization phase is to find an appropriate hull shape that minimizes the drag while placing the internal components in a clash free state minimizing the separation between centre of gravity (CG) and centre of buoyancy (CB) for better controllability. Since during the phase of optimization, the components are represented as rectangular bounding boxes, the vehicle dimensions are essentially preliminary estimates. During the phase of detailed design, the orientation of the objects and their actual geometry are considered to further modify the vehicle dimensions.

The rest of the paper is organized as follows. In Section II, a detailed description of the optimization framework and its modules is presented. Thereafter, the details of the numerical experiments are described. In Section IV, results of the optimum design are reported. Section V draws conclusions of this study.

II. Optimization Framework

The optimization framework presented in this paper consists of five applications namely Matlab, Microsoft Excel, Text Document, CATIA and VBScript. Matlab is used for numerical computation and is the basis of the whole optimization process. Microsoft Excel and Text Document are used as a medium of communication between applications. CATIA (Computer Aided Three-dimensional Interactive Application) is a multi-platform computer-aided design (CAD) software suite and widely used for design purposes. In the present study, CATIA is used for modelling the vehicle based on the geometry parameters generated from the optimization process. As the current approach utilizes the optimization modules to iterate the design of the vehicle, automation of CATIA modelling is done through a scripting language, called VBScript (Visual Basic Scripting Edition) that can generate the model without user intervention. Shown in Fig. 1 is a generic sequence diagram to illustrate the work flow of the current optimization framework.

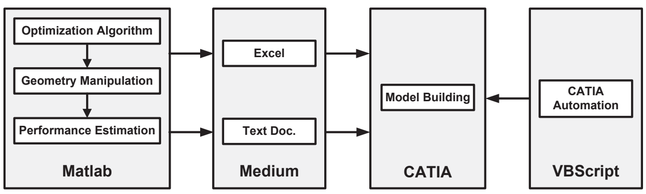

Fig. 1. Inter-process communication flow among applications

The design optimization process starts with a set of design variables that is fed into the optimization module. The optimizer generates a candidate design which translates to a hull form geometry and location of the components. The geometry and configuration modules not only generate the external hull geometry but also place the internal on-board components in a clash free state. Once the internal parts are placed in a clash free state, the parallel middle body is generated automatically covering the internal arrangement, and then nose and tail cone are attached along with the mid-body, thereby generating the complete vehicle shape. The performance of the candidate design is evaluated and used by the optimizer. These steps complete one work flow loop. The detailed flowchart of the optimization framework is presented in Fig. 2 with further discussion of this provided in subsequent sections.

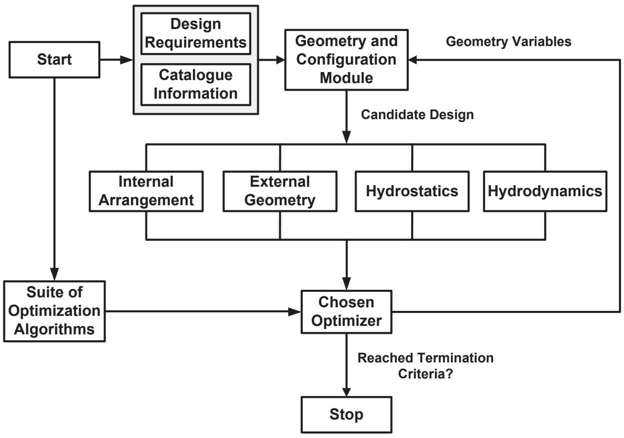

Fig. 2. Detailed flowchart of the optimization framework

A. Design Requirements

The basic design concept of the UUV employed herein is based on the development of a six inch remote controlled submarine with image capturing capability. The design process relies heavily on the use of miniature commercial-off-the-shelf (COTS) components in an attempt to contain cost. The design requirements used in this study are:

- Operating speed of the UUV is 0.2 m/s;
- Length of the UUV must be no more than 152.4 mm (6 inch);
- Should be able to house a camera of 2.87E4 mm^3 volume and radius of 19 mm;
- The vehicle is to be propelled by one rear propeller and two propellers for yaw movement. The pitch movement will be achieved through linear actuator and syringe mechanism;
- Should have enough space to carry a controller and a battery unit;
- The UUV must be able to store lead shot for ballast and weight in order to balance the buoyant force for underwater use;
- Should maintain a modular configuration for easy access to the internal components and be reconfigured to suit various mission requirements.

B. Geometry and Configuration Module

1) Hull Geometry: The hull size of the submarine is constrained by the space for the on-board instruments that are required to be carried, and the hull shape is constrained by the hydrodynamic characteristics. An axisymmetric body of revolution moving submerged near to the free surface is considered in this study. Illustration of the parameterization of the hull geometry is shown in Fig. 3, where the body comprises of a nose-section of variable length l_n, a mid-section of variable length l_m, and a tail-section of variable length l_t, making up the total body length of l units. The mid-body will hold all internal components in a clash free state, camera in the nose and thrust motor in the tail.

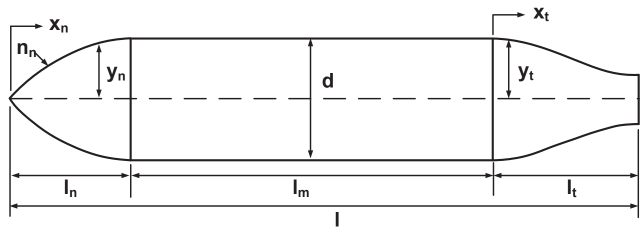

Fig. 3. Parameterization of the hull geometry

The curve shapes of the nose and tail sections are determined respectively from the Eqs. 1 and 2.

$$y_n = \frac{1}{2}d\left[1-\left(\frac{l_n - x_n}{l_n}\right)^{n_n}\right]^{\frac{1}{n_n}} \qquad (1)$$

where y_n is the radius of the nose, d is the maximum body diameter, which may be varied, l_n is the length of the nose, x_n is the reference length that varies from 0 to l_n, and n_n is the shape variation coefficient of the nose which may also be varied to give different shapes of the nose.

$$y_t = 0.0002{x_t}^3 - 0.0237{x_t}^2 + \frac{d}{2} \qquad (2)$$

where y_t is the radius of the tail and x_t is the reference length that varies from 0 to l_t.

2) Propulsion System: The submarine employs a propeller for surge control, two small propellers rotating about the vertical axis for yaw control and a hydrostatic displacement changing system for vertical displacement. This control configuration gives precise manoeuvrability and steady vertical displacement control. The internal on-board components including propulsion system for the vehicle design are shown in Fig. 4.

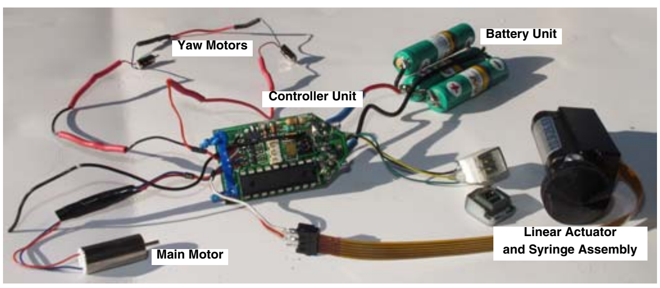

Fig. 4. Internal on-board components to be used for the vehicle design

The displacement changing system utilizes a geared stepper motor-actuated syringe mechanism which adjusts the displacement of the submarine. The syringe cavity is designed to run horizontally and positioned as far forward as possible without clashing with the camera located inside the nose to increase the induced pitch. The cavity is considered as half full at the state of neutral buoyancy as demonstrated in Fig. 5. When the syringe is extended, the face of the syringe is flush with the hull of the submarine and this state gives positive buoyancy. As the syringe face is brought back inside the submarine, the vehicle's displacement decreases and its buoyancy consequently decreases giving negative buoyancy. This change of attitude means that when the submarine tries to ascend or descend, the camera can see the direction in which it is heading and also the thrust can be used to increase the rate of ascent. Ingesting water into the syringe cavity does not adjust or raise the CG of the submarine as flooding of the cavity is treated as a loss of buoyancy rather than an addition of mass.

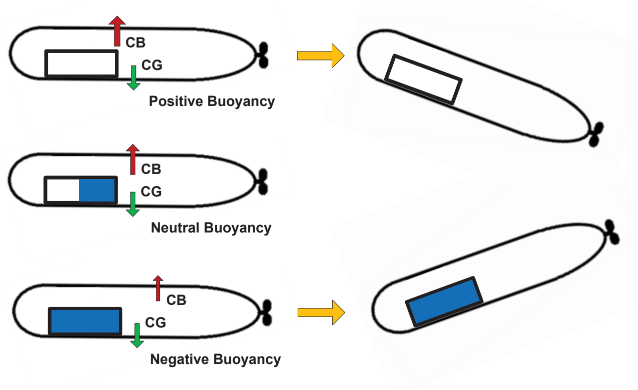

Fig. 5. Hydrostatic displacement changing system induced pitch schematic

3) Power Source: Unlike tethered vehicles, UUV operations are limited by the on board power [13]. Most underwater vehicles in use today are powered by low cost rechargeable batteries. As the present application has several design constraints such as the vehicle should be no longer than 152.4 mm, other source of power such as fuel cells and solar power are not suitable. Due to simplicity and commercial availability, we limit our selection to the consideration of primary and secondary batteries as the power source. After a careful review of the available battery systems presented by Bradley *et al.* [14], the AAA size NiMH batteries with nominal cell voltage of 3.6 V are proven to be the best option for the power source of the present application. They also meet the vehicle size constraints.

4) Arrangement of Internal Components: The design optimization framework not only optimizes the hull shape but also arranges its contents avoiding interference while maintaining workable spaces around the components using 'clash free mechanism'. For efficient utilization of the available internal volume, a careful arrangement needs to be achieved. While in reality some components have irregular shapes, minimum bounding box dimensions have been used to derive the clash free configuration. Details of the clash free mechanism appear in Alam *et al.* [15].

5) Control Module: When designing such a small scale UUV with mostly off-the-shelf components, it is important to establish which component will be most restrictive in size and shape as this component will more than likely determine one or more of the minimum geometric constraints. Considering the aforementioned design constraints, it is decided to use the remote control and circuitry system of the *Emden U16* [7] as shown in Fig. 4, for the current application. The circuitry of the U16 incorporates a 3 channel remote control which provides a positive or negative polarity to three separate circuits. That is, one circuit for each degrees of freedom (linear actuator, main motor and yaw control motors). This remote provides intuitive control of the submarine operating at 27 MHz.

The image capturing capability of the UUV is achieved by a standalone digital video recording (DVR) 'spy' camera which will be positioned forward most for visibility. The camera is the most restrictive component that dictated the diameter of the UUV. Several 'spy' type cameras have investigated and the 'micro eyes ball camera' is selected for the current design. The selected ball camera is spherical in shape and fits easily within the nose section without interfering the components located at the parallel mid-body.

C. Optimization Module

The design optimization framework is embedded with a suite of state-of-the-art optimization algorithms, the non-dominated sorting genetic algorithm II (NSGA-II) [16], infeasibility driven evolutionary algorithm (IDEA) [17] and infeasibility empowered memetic algorithm (IEMA) [18]. It is worth mentioning that any optimization algorithm capable of solving single and multi-objective optimization problems can be used within the framework.

Since in reality, solutions to constrained optimization problems such as those presented in the following section of this paper are expected to lie on constraint boundaries, the notion of preserving *infeasible solutions* is known to accelerate the rate of convergence. The infeasible solution refers to the solution that violates one or more of the constraints during optimization while achieving a better objective value. The concept of IDEA was introduced by the second author of this paper and has been used in this study for optimum design of underwater vehicles.

IDEA tries to focus the search near the constraint boundaries by maintaining a set of infeasible solutions in addition to feasible solutions. It ranks the infeasible solutions higher than the feasible solutions to provide a selection pressure to create *better* infeasible solutions resulting in an active search through the infeasible search space. In addition, the set of marginally infeasible solutions obtained using IDEA, may also be useful for trade-off studies for engineering design problems. The details on the algorithm can be found from the works of Ray *et al.* [19].

D. Analysis Module: Drag Estimation

The hull for the design vehicle has been optimized for minimum drag that eventually reduces the submerged vehicle power requirements [20]. For drag estimation, the following formula has been used:

$$D = \frac{1}{2}\rho V^2 C_V S \tag{3}$$

where ρ is the density of the fluid, V is the velocity, S is the wetted surface area of the vehicle, C_V is the coefficient of viscous resistance for the smooth bare hull and D is the vehicle drag.

Three methods- Virginia Tech (VT) [21], MIT [22] and G&J method [23] are employed in this study to measure the coefficient of viscous resistance (C_V) in three different ways to ensure uniformity in drag estimation of the design vehicle. The optimization process involves a search through a large variable space in the presence of highly nonlinear constraints arising out of design requirements with an aim to reduce drag.

III. Numerical Experiment

In this section, the formulation of the optimization problem based on the design requirements is presented. The significance of various design criteria are also further discussed.

A. Single Objective Optimization Problem Definition

The single objective optimization problem posed can be described as the identification of a vehicle hull form with minimum drag as well as clash free optimal placement of the internal objects subject to the constraints on length and diameter of the vehicle, lever arms and CG-CB separation. The first (LA_1) and second (LA_2) lever arms are the longitudinal distances of the yaw propellers from the centre of buoyancy respectively. The higher value of lever arm produces higher turning moments that lead to better heading changes. The lower the value of CG-CB separation (s), the closer the position of the CG and CB that leads to better stability of the vehicle. Constraints on overall length (l) and diameter (d) of the vehicle are also important to meet the basic design requirements. Constraints have also applied for the inner diameter (ID_n) and inner volume (IV_n) of the nose so that it can house the camera properly. Minimization of drag (D) is important because minimum drag leads to least power consumption for propulsion, and corresponding savings in the operating costs.

The design variables of the problem as illustrated in Fig. 6 are the positions of the internal components along the X, Y and Z axes, the nose and tail parameters. The mathematical model of the optimization problem is stated in Eq. (4).

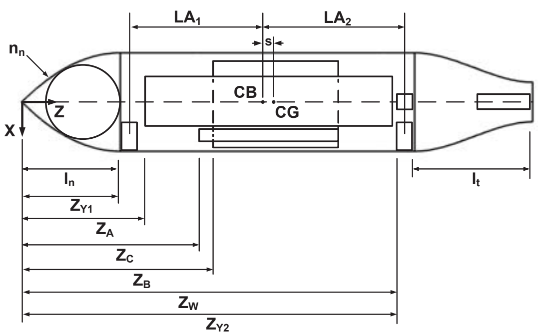

Fig. 6. The constraints and design variables for problem formulation

$$
\begin{array}{l}
\text{Minimize:} \\
f(1) = D \\
\\
\text{Subject to:} \\
g(1) = l \leq 152.4\ mm;\quad g(2) = l/d \geq 2.8 \\
g(3) = LA_1 \geq 35\ mm;\quad g(4) = LA_2 \geq 35\ mm \\
g(5) = s \leq 4\ mm;\quad g(6) = ID_n \geq 38\ \ mm \\
g(7) = IV_n \geq 2.8742E4\ \ mm^3 \\
\\
\text{Variable bounds:} \\
0 \leq X_A \leq 50\ mm;\ 0 \leq Y_A \leq 50\ mm;\ 0 \leq Z_A \leq 50\ mm \\
0 \leq X_B \leq 50\ mm;\ 0 \leq Y_B \leq 50\ mm;\ 0 \leq Z_B \leq 50\ mm \\
0 \leq X_C \leq 50\ mm;\ 0 \leq Y_C \leq 50\ mm;\ 0 \leq Z_C \leq 50\ mm \\
0 \leq X_W \leq 50\ mm;\ 0 \leq Y_W \leq 50\ mm;\ 0 \leq Z_W \leq 50\ mm \\
0 \leq X_{Y1} \leq 50\ mm;\ 0 \leq Y_{Y1} \leq 50\ mm;\ 0 \leq Z_{Y1} \leq 50\ mm \\
0 \leq X_{Y2} \leq 50\ mm;\ 0 \leq Y_{Y2} \leq 50\ mm;\ 0 \leq Z_{Y2} \leq 50\ mm \\
2 \leq n_n \leq 3;\ 40 \leq l_n \leq 45\ mm \\
30 \leq l_t \leq 35\ mm
\end{array}
\tag{4}
$$

B. Computational Setup

For the above formulated problem, 30 independent runs using IDEA are performed, as carrying out multiple runs is a usual practice in the field of evolutionary computation. Results are presented based on these multiple runs by varying the seed value while keeping the other parameters like crossover probability, mutation probability, crossover distribution index and mutation distribution index constant for all runs. The values of the parameters are listed in Table I.

TABLE I

Parameters used for the experiment

Parameter	Value
Population size	300
Maximum function evaluations	60000
Crossover probability	0.9
Crossover distribution index	10
Mutation probability	0.1
Mutation distribution index	20
Infeasibility ratio (α)	0.2

IV. Results and Discussion

In this study evaluations are collected from the numerical experiments by the Matlab software. The computing time per evaluation (without invoking CATIA) is about 0.05 s in an Intel Xeon processor machine of 3.33 GHz with 6.00 GB memory.

A. Single Objective Optimization Results

Shown in Fig. 7 is the result of the best run for the single objective drag minimization problem using IDEA. The feasibility ratio of the best run is 0.688.

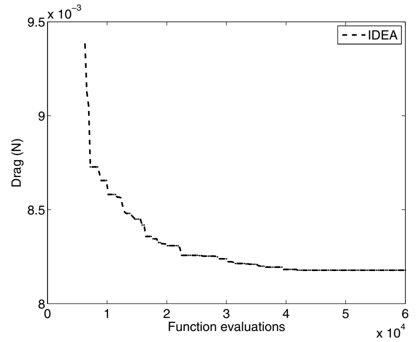

Fig. 7. Progress plot of the best design for single objective drag minimization using IDEA

It can be observed from the Fig. 7 that the optimization algorithm is able to reduce the drag around 15% as compared to initial value in 40,000 function evaluations. The values such as mean, median and standard deviation (SD) computed across 30 runs are reported in Table II. The results clearly indicate the consistency of the underlying algorithm of the optimization framework along multiple runs. Shown in Fig. 8 is a typical initial solution of the best run.

B. Results of the Preliminary μUUV Design

Based on the results obtained by carrying out an optimization exercise, Figs. 9 and 10 show the best shape and internal configuration of the preliminary design. The values of the design variables for the preliminary design are presented in Table III. It is important to note that the nose length needs

TABLE II
SINGLE OBJECTIVE DRAG MINIMIZATION RESULTS

Drag	IDEA
Best	0.0081782 N
Mean	0.0081782 N
Median	0.0081782 N
Worst	0.0081830 N
SD	9.12871E-7

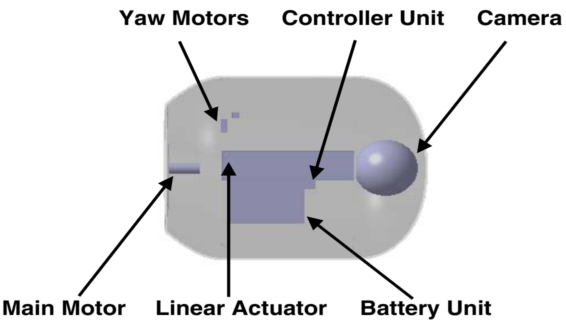

Fig. 8. Configuration of a typical initial solution

to be added with the $Z-$coordinates of the internal units in order to obtain the actual positions from the nose-tip.

Fig. 9. Bare hull of the preliminary design

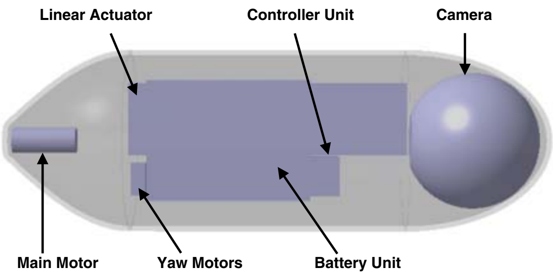

Fig. 10. Internal configuration of the preliminary design

TABLE III
DERIVED QUANTITIES OF THE DESIGN VARIABLES FOR THE PRELIMINARY DESIGN

Variable	Lower	Upper	Best	Variable	Lower	Upper	Best
X_A	0	50	27.51	Y_A	0	50	17.86
Z_A	0	50	45.53	X_B	0	50	27.04
Y_B	0	50	42.86	Z_B	0	50	39.55
X_C	0	50	47.99	Y_C	0	50	18.38
Z_C	0	50	31.27	X_W	0	50	49.88
Y_W	0	50	27.85	Z_W	0	50	39.20
X_{Y1}	0	50	49.50	Y_{Y1}	0	50	48.66
Z_{Y1}	0	50	40.17	X_{Y2}	0	50	49.71
Y_{Y2}	0	50	33.87	Z_{Y2}	0	50	41.11
n_n	2	3	2	l_n	40	45	40.00
l_t	30	35	34.40				

The resulting performance criteria of the preliminary best design are listed in Table IV. The values of the lever arms, CG-CB separation, length and diameter of the vehicle clearly indicate that the design constraints are satisfied while achieving minimum drag.

C. Detailed Design of the μUUV

The focus of the detailed design is to finalize the preliminary design with the actual components to be built. In this step of the UUV design, all the actual on-board components are placed in their respective positions as obtained from the best solution of the optimization exercise. In order to verify the design and move the data into a useful form, CATIA is used to show the location of the components and a visual representation of the vehicle itself as illustrated in Fig. 11. This ensures that the process has operated correctly and the design is feasible to be built.

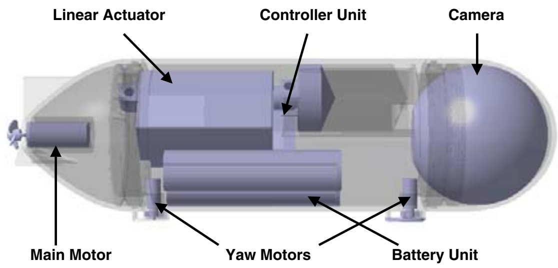

Fig. 11. Internal configuration of the final design

It is important to note that the clash free mechanism adopted in the present study, despite the fact that the internal components are not necessarily rectangular, they are represented as the minimum *bounding boxes*. Another limitation of the current approach is the inadequacy of *rotated* placement of the on-board components. These obviously limit the way in which the objects can be placed together. The detailed design demonstrates and provides a tighter assembly yet clash-free. The major consequence of this CAD analysis is the reduced diameter of the final design, and a lower drag of the submarine as compared to preliminary design that reported in Table IV.

It is worth highlighting that for detailed design, no optimization exercise has been carried out. The preliminary design identified through the process of optimization provides the design boundaries for the detailed design phase. A detailed CAD based analysis using CATIA is carried out in the detailed design phase. The actual shapes of the on-board components are drawn prior to the analysis. To compute the drag of the final design, a Matlab function is used (the same function used during the course of optimization).

D. Computational Fluid Dynamics Analysis

The computational fluid dynamics (CFD) analysis is becoming more and more popular in estimating the hydrodynamic parameters such as drag, although it is computationally more expensive than the empirical ones [24]. CFD can provide accurate simulations of the flow around the vehicle, and a useful understanding of the fluid-structure interactions [25]. Therefore a 3D CFD analysis for a better drag estimation has been carried out following the optimization approach.

1) Theoretical Background of the CFD Analysis: The numerical analysis of flow around submerged bodies is based on the incompressible Navier-Stokes equations that describe the flow properties such as the velocity, pressure,

TABLE IV

PERFORMANCE CRITERIA OF THE PRELIMINARY AND DETAILED DESIGNS

Vehicle particulars	Preliminary	Detailed
Nose length	40 mm	36 mm
Parallel middle body length	78 mm	81 mm
Tail length	34.40 mm	30 mm
Length overall	152.40 mm	147 mm
Maximum diameter	51.10 mm	42 mm
Length to diameter ratio	2.98	3.5
Maximum dimension of the inner square	34.02 mm	27.58 mm
Wetted surface area	0.021611 m^2	0.018611 m^2
Displacement volume	0.000247 m^3	0.0001698 m^3
Mass of the displaced water	247 g	169.8 g
Total mass of the vehicle	172.17 g	150 g
Length of the first lever arm	37.44 mm	30.87 mm
Length of the second lever arm	38.41 mm	39.13 mm
X-coordinate of CG	0.945431 mm	-1.649 mm
Y-coordinate of CG	1.60895 mm	-0.146 mm
Z-coordinate of CG	72.3486 mm	71.27 mm
X-coordinate of CB	0	-0.03 mm
Y-coordinate of CB	0	0.009 mm
Z-coordinate of CB	76.2258 mm	70.868 mm
Longitudinal distance between CB and CG	3.8772 mm	0.402 mm
Nominal speed	0.2 m/s	0.2 m/s
Drag (VT method)	0.0063382 N	0.0052760 N
Drag (G&J method)	0.0067334 N	0.0055610 N
Drag (MIT method)	0.0081782 N	0.0063863 N

temperature and density. Discretizing the equations with respect to time produces the Reynolds Averaged Navier-Stokes (RANS) equations that are commonly used in most commercially available CFD packages. The commercial CFD software package ANSYS 13.0 has been used in the current study to simulate the flow around the designed vehicles.

2) Model Building and Flow Domain: The bare hull shape is drawn in CATIA based on the hull parameters and exported to ICEM CFD as a *step* file for meshing. As the object is axisymmetric, quarter model of the bare hull is considered for CFD analysis to reduce the computational costs. The computational far field is extended $16l$ upstream of the leading edge, $18l$ downstream from the trailing edge and $10l$ above the body surface, where l being the length of the vehicle. Since the flow is incompressible, the considered solution domain is found large enough to capture the entire viscous-inviscid interaction and the wake development.

3) Grid Generation: After defining the model and the far field, the solution domain is decomposed into appropriate number of locations based on the accuracy of the results required. Geometry meshing in this study is generated by using ANSYS ICEM CFD Meshing software. The mesh file is then exported to FLUENT for numerical study. The generated mesh is composed primarily of tetrahedral elements. Typically in total $180,776$ regular elements were built with $64,785$ nodes in the solution domain.

In flow simulations using the turbulence models, the computational grid should be in such a way that sufficient number of grid points lie within the laminar sublayer of the ensuing boundary layer [26]. Therefore 'prism' elements with 50 layers are selected for generating meshes adjacent to the body surfaces as these are the most appropriate for a boundary layer mesh [27]. Also to capture the wake, dense mesh are selected near the stern of the vehicle body as illustrated in Fig. 12.

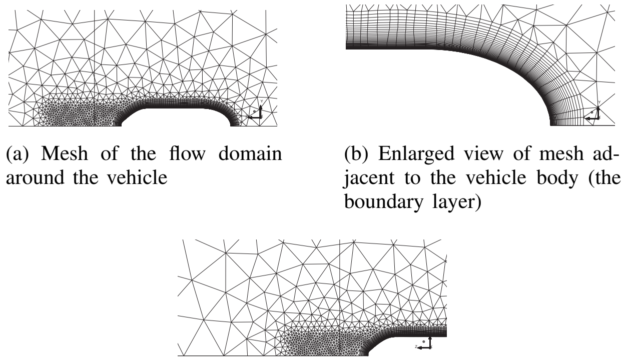

(a) Mesh of the flow domain around the vehicle

(b) Enlarged view of mesh adjacent to the vehicle body (the boundary layer)

(c) Enlarged view of dense mesh near the stern side

Fig. 12. Generated mesh highlighting the boundary layer grid adjacent to the vehicle body

4) Problem Setup and Simulation: When the computational domain is meshed, the flow is solved using the software ANSYS FLUENT 13.0. The Reynolds numbers of the surrounding flow of the vehicle is typically 3.04×10^4. From the various turbulence models, the realizable $k - \varepsilon$ model with enhanced wall treatment is applied to simulate the surrounding flow of the vehicle. This model is quite robust, economic and reasonably accurate for a wide range of turbulent flows [27].

5) Results of CFD Analysis: The drag values obtained for the preliminary and detailed designs computed using ANSYS (FLUENT) under turbulence flow regimes with flow speed of 0.2 m/s are presented in Table V. The values of drag force obtained from both empirical and CFD methods as reported in Table V show good agreement. Thus the ranking of the designs are consistent with the values obtained using the empirical relations.

TABLE V

COMPARISON OF DRAG VALUES BETWEEN EMPIRICAL AND CFD ESTIMATES

Design	Empirical method	CFD analysis
Preliminary	0.0081782 N	0.0104007 N
Detailed	0.0063863 N	0.0082638 N

Other than drag estimation, the CFD analysis is also performed with the purpose of obtaining the pressure and velocity distributions around the vehicle under the influence of streaming water. Shown in Fig. 13 is a visualization of the pressure distribution of the flow around the body of the designed vehicles. An even distribution of pressure can be seen along the main body except for the stagnation point at the nose-tip of the hull. The pressures at the nose and tail sections are higher compared to the pressure along the main body of the UUV.

The velocity contours of flow around the surfaces of the designed vehicles are shown in Fig. 14. It can be seen that the velocity around the nose is lower and the flow is accelerated as it reaches the stern. This can be explained from the conservation of energy, in a steady flow, an increase in the pressure of the fluid occurs simultaneously with a decrease in the velocity. As the pressure at the nose of the UUV is higher, therefore the velocity is lower at this region. As the outlet gauge pressure is set to zero and also due to the shape

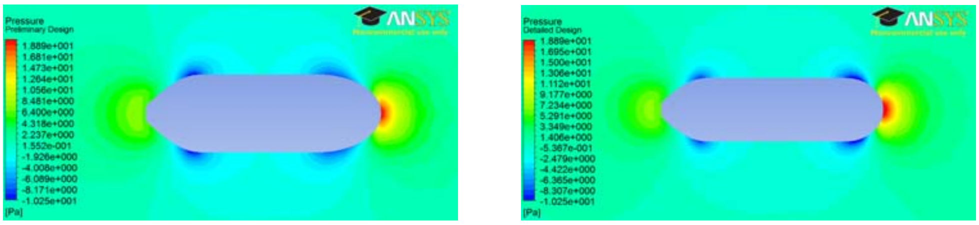

(a) Preliminary design

(b) Detailed design

Fig. 13. Pressure contours around the surfaces of the designed vehicles

of tail, the flow-stream converges when it reaches to the stern and velocity increases.

E. Fabrication

The fabrication phase includes the development of a tooling and manufacturing process aimed at ensuring accurate, viable and efficient construction of the individual modules. The components of the hull illustrated in Fig. 15(a) are rapid prototyped using a 3D printer available in the School of Engineering and Information Technology, UNSW Canberra which are not *off-the-shelf* components. With all on-board components acquired, the assembly begins with the linear actuator as this is the largest individual component and requires the most room to manoeuvre into position. Then the electronics including battery unit are installed inside the mid-body. Each of the motors are then inserted into their respective mounting holes and a substantial bead of black silicone is used to seal the motors against the hull to prevent water ingress. To seal the UUV, O-rings are fitted along the dividing lines with a thin coat of silicone grease to aid sealing. Finally to complete the assembly as shown in Fig. 15(d), all that required is to place the camera inside the nose, apply some silicone grease to the O-rings and connect the nose section to the mid-body.

Performance testing is conducted in a large fish tank and depicted in Fig. 15(e). The vehicle is trimmed to neutral buoyancy and balanced to sit horizontally leveled in the water using small bags of lead shot. The vehicle proves to be precisely manoeuvrable, demonstrating operating speed of approximately 0.2 m/s, rotating with zero turn radius and diving and surfacing at an approximate rate of 0.05 m/s.

V. Conclusions

There is an increasing interest in design and development of mini/micro UUVs that are nominally less than one foot in length. In this paper, an efficient evolutionary approach is introduced for the preliminary design of μUUVs. The ability of the approach to represent and optimize a class of μUUV is illustrated through designing a torpedo-shaped miniature UUV with an overall length of six inches. Furthermore the design process relies heavily on the use of off-the-shelf components to contain both risk and cost. The use of an efficient integrated analysis/design system comprising Matlab and CAD package (CATIA), the framework is able to generate an optimized geometry of the UUV based on given design requirements.

The current approach is embedded with a clash free mechanism that relies on the minimum rectangular bounding box dimensions, despite the irregular shapes of the internal on-board components. In an attempt to enhance the performance of the preliminary design, a detailed CAD analysis has been carried out that overcomes the limitations of the present approach and make the design viable to be built. The preliminary and detailed designs are also validated using CFD analyses to establish confidence on the empirical estimates used during the course of optimization. The final design is then built to resolve remaining uncertainties in the design and tested in a large fish tank. The UUV met the specified design requirements and successfully demonstrated the concept of a six inch remote controlled UUV with image capturing capability.

Appendix A. Notation

D	Drag
d	Maximum body diameter
ID_n	Inner diameter of the nose
IV_n	Inner volume of the nose
l	Length overall
l_m	Length of the parallel middle body
l_n	Length of the nose
l_t	Length of the tail
LA_1	Length of the first lever arm
LA_2	Length of the second lever arm
n_n	Shape variation coefficient of the nose
s	Longitudinal distance between CB and CG
X_A, Y_A, Z_A	Coordinates of the actuator unit
X_B, Y_B, Z_B	Coordinates of the battery unit
X_C, Y_C, Z_C	Coordinates of the controller unit
X_W, Y_W, Z_W	Coordinates of the dead weight
X_{Y1}, Y_{Y1}, Z_{Y1}	Coordinates of the first yaw motor
X_{Y2}, Y_{Y2}, Z_{Y2}	Coordinates of the second yaw motor

Acknowledgments

The first author would like to acknowledge the Research Publication Fellowship he received from the University of New South Wales, Canberra, Australia. The second author would like to acknowledge the support of Future Fellowship offered by the Australian Research Council.

References

[1] J. Yuh, "Design and control of autonomous underwater robots: A survey," *Autonomous Robots*, vol. 8, pp. 7–24, 2000.

[2] K. Alam, T. Ray, and S. G. Anavatti, "Design of a toy submarine using underwater vehicle design optimization framework," in *Computational Intelligence in Vehicles and Transportation Systems (CIVTS), 2011 IEEE Symposium on*, Paris, France, 2011, pp. 23 –29.

[3] S. Watson and P. Green, "A de-coupled vertical controller for micro-autonomous underwater vehicles (μAUVs)," in *Mechatronics and Automation (ICMA), 2011 International Conference on*, 2011, pp. 561–566.

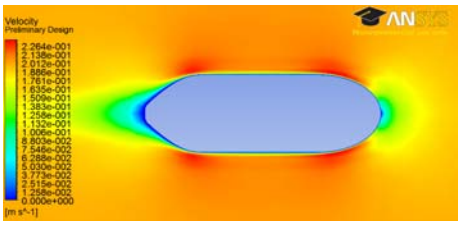

(a) Preliminary design

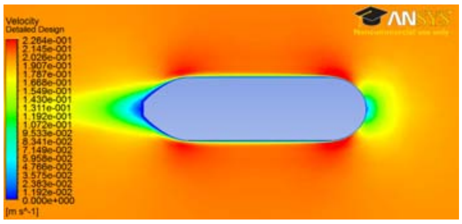

(b) Detailed design

Fig. 14. Velocity contours around the surfaces of the designed vehicles

(a) Hull components

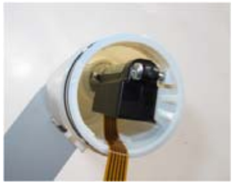

(b) Mid-body with linear actuator installed

(c) Mid-body with all internal components installed

(d) Prototype: six inch submarine

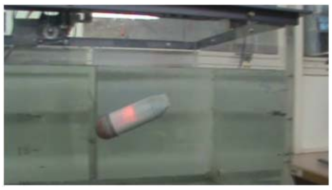

(e) UUV in operation during testing

Fig. 15. Fabrication of the μUUV

[4] R. Lopez, I. Torres, J. Escareo, S. Salazar, and A. Palomino, "Quad-tilting thrusters micro submarine: Modeling and control of the attitude," in *Electronics, Communications and Computer (CONIELECOMP), 2010 20th International Conference on*, 2010, pp. 85–89.

[5] S. Watson and P. Green, "Propulsion systems for micro-Autonomous Underwater Vehicles (μAUVs)," in *Robotics Automation and Mechatronics (RAM), 2010 IEEE Conference on*, 2010, pp. 435–440.

[6] V. Kopman, N. Cavaliere, and M. Porfiri, "MASUV-1: A Miniature Underwater Vehicle With Multidirectional Thrust Vectoring for Safe Animal Interactions," *Mechatronics, IEEE/ASME Transactions on*, vol. 17, no. 3, pp. 563–571, 2012.

[7] J. Fearnley and T. Ray, "Design and development of a six inch sub," in *Submarine Institute of Australia Science, Technology & Engineering Conference 2011, Adelaide, Australia*, 2011, pp. 273–279.

[8] P. Kodati, J. Hinkle, and X. Deng, "Micro Autonomous Robotic Ostraciiform (MARCO): Design and Fabrication," in *Robotics and Automation, 2007 IEEE International Conference on*, 2007, pp. 960–965.

[9] D. Walker, "Micro autonomous underwater vehicle concept for distributed data collection," in *OCEANS 2006 IEEE*, 2006, pp. 1–4.

[10] F. Bruhn, F. Carsey, J. Kohler, M. Mowlem, C. German, and A. Behar, "MEMS enablement and analysis of the miniature autonomous submersible explorer," *Oceanic Engineering, IEEE Journal of*, vol. 30, no. 1, pp. 165–178, 2005.

[11] A. Gadre, J. Mach, D. Stilwell, and C. Wick, "Design of a prototype miniature autonomous underwater vehicle," in *Intelligent Robots and Systems, 2003, (IROS 2003), IEEE/RSJ International Conference on*, vol. 1, 2003, pp. 842–846.

[12] B. Hobson, B. Schulz, J. Janet, M. Kemp, R. Moody, C. Pell, and H. Pinnix, "Development of a micro autonomous underwater vehicle for complex 3-D sensing," in *OCEANS, 2001, MTS/IEEE Conference and Exhibition*, vol. 4, 2001, pp. 2043–2045.

[13] V. P. Shah, "Design considerations for engineering autonomous underwater vehicles," Master's thesis, Massachusetts Institute of Technology, June 2007.

[14] A. M. Bradley, M. D. Feezor, H. Singh, and F. Y. Sorrell, "Power Systems for Autonomous Underwater Vehicles," *IEEE Journal of Oceanic Engineering*, vol. 26, no. 4, pp. 526–538, 2001.

[15] K. Alam, T. Ray, and S. G. Anavatti, "A new robust design optimization approach for unmanned underwater vehicle design," *Proceedings of the Institution of Mechanical Engineers, Part M: Journal of Engineering for the Maritime Environment*, vol. 226, no. 3, pp. 235–249, 2012.

[16] K. Deb, A. Pratap, S. Agarwal, and T. Meyarivan, "A Fast and Elitist Multiobjective Genetic Algorithm: NSGA-II," *IEEE Transactions on Evolutionary Computation*, vol. 6, no. 2, pp. 182–197, 2002.

[17] H. K. Singh, A. Isaacs, T. Ray, and W. Smith, "Infeasibility Driven Evolutionary Algorithm (IDEA) for Engineering Design Optimization," in *21st Australasian Joint Conference on Artificial Intelligence: Advances in Artificial Intelligence, Auckland, New Zealand, Springer-Verlag Berlin Heidelberg*, no. LNAI 5360, 2008, pp. 104–115.

[18] H. K. Singh, T. Ray, and W. Smith, "Performance of Infeasibility Empowered Memetic Algorithm (IEMA) on Engineering Design Problems," in *Australasian Conference on Artificial Intelligence'2010*, 2010, pp. 425–434.

[19] T. Ray, H. K. Singh, A. Isaacs, and W. Smith, *Infeasibility Driven Evolutionary Algorithm for Constrained Optimization*, E. Mezura-Montes, Ed. Springer Berlin / Heidelberg, 2009, vol. 198.

[20] J. S. Parsons, R. E. Goodson, and F. R. Goldschmied, "Shaping of axisymmetric bodies for minimum drag in incompressible flow," *J. Hydronautics*, vol. 8, no. 3, pp. 100–107, 1974.

[21] M. A. Martz, "Preliminary design of an autonomous underwater vehicle using a multiple-objective genetic optimizer," Master's thesis, Virginia Polytechnic Institute and State University, Blacksburg, Virginia, United States, May 27 2008.

[22] H. A. Jackson, "MIT Professional Summer Course Submarine Design Trends," 1992.

[23] T. Gillmer and B. Johnson, *Introduction to Naval Architecture*, 2nd ed. US Naval Institute Press, 1982.

[24] M. Martz and W. L. Neu, "Multi-objective optimization of an autonomous underwater vehicle," *Marine Technology Society Journal*, vol. 43, no. 2, 2009.

[25] R. P. Irwin and C. Chauvet, "Quantifying hydrodynamic coefficients of complex structures," in *Proceedings of the OCEANS 2007, Aberdeen, UK*, 2007.

[26] M. M. Karim, M. M. Rahman, and M. A. Alim, "Numerical computation of viscous drag for axisymmetric underwater vehicles," *Jurnal Mekanikal*, vol. 26, pp. 9–21, 2008.

[27] T. Joung, K. Sammut, F. He, and S.-K. Lee, "A Study on the Design Optimization of an AUV by Using Computational Fluid Dynamic Analysis," in *Proceedings of the Nineteenth (2009) International Offshore and Polar Engineering Conference, Osaka, Japan*, 2009, pp. 696–702.